



NAVAL POSTGRADUATE SCHOOL

MONTEREY, CALIFORNIA

MODAL TESTING OF THE NPSAT1 ENGINEERING

DEVELOPMENT UNIT

by

Sajoscha Rahn

July 2012

Approved for public release; distribution unlimited.

THIS PAGE INTENTIONALLY LEFT BLANK

REPORT DOCUMENTATION PAGE				Form Approved OMB No. 0704-0188	
Public reporting burden for this collection of information is estimated to average 1 hour per response, including the time for reviewing instructions, searching existing data sources, gathering and maintaining the data needed, and completing and reviewing this collection of information. Send comments regarding this burden estimate or any other aspect of this collection of information, including suggestions for reducing this burden to Department of Defense, Washington Headquarters Services, Directorate for Information Operations and Reports (0704-0188), 1215 Jefferson Davis Highway, Suite 1204, Arlington, VA 22202-4302. Respondents should be aware that notwithstanding any other provision of law, no person shall be subject to any penalty for failing to comply with a collection of information if it does not display a currently valid OMB control number. PLEASE DO NOT RETURN YOUR FORM TO THE ABOVE ADDRESS.					
1. REPORT DATE (DD-MM-YYYY) 28-09-2012		2. REPORT TYPE Technical Report		3. DATES COVERED (From-To)	
4. TITLE AND SUBTITLE Modal Testing of the NPSAT1 Engineering Development Unit				5a. CONTRACT NUMBER	
				5b. GRANT NUMBER	
				5c. PROGRAM ELEMENT NUMBER	
6. AUTHOR(S) Sajoscha Rahn				5d. PROJECT NUMBER	
				5e. TASK NUMBER	
				5f. WORK UNIT NUMBER	
7. PERFORMING ORGANIZATION NAME(S) AND ADDRESS(ES) Naval Postgraduate School Monterey, CA				8. PERFORMING ORGANIZATION REPORT NUMBER NPS-SP-12-001	
9. SPONSORING / MONITORING AGENCY NAME(S) AND ADDRESS(ES)				10. SPONSOR/MONITOR'S ACRONYM(S)	
				11. SPONSOR/MONITOR'S REPORT NUMBER(S)	
12. DISTRIBUTION / AVAILABILITY STATEMENT Approved for public release; distribution unlimited					
13. SUPPLEMENTARY NOTES The views expressed in this thesis are those of the author and do not reflect the official policy or position of the Department of Defense or the U.S. Government.					
14. ABSTRACT The purpose of this thesis is to validate a finite element model of the small satellite NPSAT1. A-modal test of this satellite will be conducted and the results will be correlated to the FEM simulation results. Furthermore, this thesis provides an overview of modal parameter extraction techniques and the theories behind them. Impact testing is chosen to obtain the data. In the end, the FEM is found to be inaccurate and suggestions are presented for improvements.					
15. SUBJECT TERMS					
16. SECURITY CLASSIFICATION OF:			17. LIMITATION OF ABSTRACT UU	18. NUMBER OF PAGES 58	19a. NAME OF RESPONSIBLE PERSON Dan Sakoda
a. REPORT UNCLASSIFIED	b. ABSTRACT UNCLASSIFIED	c. THIS PAGE UNCLASSIFIED			19b. TELEPHONE NUMBER (include area code) 831-656-3198

Standard Form 298 (Rev. 8-98)
Prescribed by ANSI Std. Z39.18

THIS PAGE INTENTIONALLY LEFT BLANK

NAVAL POSTGRADUATE SCHOOL
Monterey, California 93943-5000

Daniel T. Oliver
President

Leonard A. Ferrari
Executive Vice President and
Provost

The report entitled “*Modal Testing of the NPSAT1 Engineering Development Unit*” was prepared for the Naval Postgraduate School Space Systems Academic Group.

Further distribution of all or part of this report is authorized.

This report was prepared by:

Sajoscha Rahn,
Lt. z. S, German Navy

Reviewed by:

Rudolf Panholzer,
Chairman
Space Systems Academic Group

Released by:

Jeffrey D. Paduan
Vice President and
Dean of Research

THIS PAGE INTENTIONALLY LEFT BLANK

ABSTRACT

The purpose of this thesis is to validate a finite element model of the small satellite NPSAT1. A modal test of this satellite will be conducted and the results will be correlated to the FEM simulation results. Furthermore, this thesis provides an overview of modal parameter extraction techniques and the theories behind them. Impact testing is chosen to obtain the data. In the end, the FEM is found to be inaccurate and suggestions are presented for improvements.

THIS PAGE INTENTIONALLY LEFT BLANK

DECLARATION

I hereby declare that this thesis has been created by myself using only the named sources and supplementary equipment.

ERKLÄRUNG

Hiermit erkläre ich, dass die vorliegende Master Arbeit von mir selbstständig und nur unter Verwendung der angegebenen Quellen und Hilfsmittel angefertigt wurde.

Monterey, 01. August 2012

Sajoscha Rahn, Lt. z. S.

THIS PAGE INTENTIONALLY LEFT BLANK

TABLE OF CONTENTS

I. INTRODUCTION	1
II. THEORY OF MODAL ANALYSIS.....	3
A. BASIC CHECK OF DATA.....	3
1. Low-frequency asymptotes	3
2. Mode Indicator Functions (MIFs)	4
B. PARAMETER EXTRACTION	6
1. SDOF Modal Analysis Methods	7
a) <i>Peak-Picking Method</i>	8
b) <i>Circle-Fit Method</i>	9
c) <i>Residual Terms</i>	11
2. MDOF Modal Analysis Methods	13
a) <i>Complex Exponential Method</i>	13
b) <i>Rational Fraction Polynomial Method</i>	16
C. CORRELATING TEST RESULTS AND SIMULATION RESULTS	19
1. Frequency Response Assurance Criterion.....	19
2. Modal Assurance Criterion.....	19
III. MODAL TESTING OF NPSAT1	23
A. TEST SETUP	23
B. MEASUREMENTS	24
C. MODAL ANALYSIS	25
1. Peak-Picking Method on NPSAT1 Data	25
2. Circle Fit Analysis of NPSAT1.....	27
3. Complex Exponential Analysis of NPSAT1 in Frequency Domain	30
4. Rational Fraction Polynomial Analysis of NPSAT1	32
IV. CONCLUSION AND OUTLOOK.....	37
V. LIST OF REFERENCES	41

THIS PAGE INTENTIONALLY LEFT BLANK

LIST OF FIGURES

Figure 1: Expanded View of NPSAT1	2
Figure 2: Complex Mode Indicator Function (CMIF)	5
Figure 3: Multivariate Mode Indicator Function (MMIF)	6
Figure 4: Nyquist plot of FRF	10
Figure 5: Example of Stability Diagram	16
Figure 6: Example of Stability Diagram MIF Overlay	17
Figure 7: Example of Frequency Shift	18
Figure 8: Example of 3D and 2D Presentation of MAC	21
Figure 9: Test Setup Free Boundary Conditions and Computer Model	24
Figure 10: Fixed Accelerometers	24
Figure 11: FRF Ref: 123X-; Res: 11X+	26
Figure 12: Circle Fit Nyquist Plot Response 11X+ Reference 123X-	28
Figure 13: Circle Fit Single Mode Curve Fit	28
Figure 14: 3D Animation of Mode 14 Using Circle Fit Method	29
Figure 15: Complex Exponential Mode Selection Z-Reference	31
Figure 16: Stability Diagram RFP Global X-Reference	33
Figure 17: Cluster Diagram RFP Local X-Reference	34
Figure 18: Point Mobility FRF Ref: 123X-	37
Figure 19: MAC Simulation vs. RFP local X-Reference	38
Figure 20: 3D MAC Simulation vs. RFP local X-Reference	38

THIS PAGE INTENTIONALLY LEFT BLANK

LIST OF TABLES

Table 1: Example of Numerical Presentation of MAC	21
Table 2: Mode Table Using Peak-Picking Method	27
Table 3: Circle-Fit Results	30
Table 4: Modal Parameters Using Complex Exponential Technique	32
Table 5: Mode Table using RFP Global Solution	33
Table 6: Mode Table Using RFP Local Solution.....	35

THIS PAGE INTENTIONALLY LEFT BLANK

NOTATION

$[...]$	matrix
$\{...\}$	vector
$[...]^T$	transpose of matrix
$[...]^H$	Hermitian (transpose complex conjugate) of matrix
$[...]^*$	complex conjugate of matrix
${}_sA_{jk}$	modal constant
$H_{jk}(\omega)$	individual frequency response function element between coordinates j and k (response at j due to excitation at k)
$h_{jk}(\omega)$	individual impulse response function element between coordinates j and k (response at j due to excitation at k)
i	$\sqrt{-1}$
m	number of included modes
N	total number of modes
$\alpha_{jk}(\omega)$	dynamic compliance or receptance
ζ	viscous damping
η	structural damping
ψ	mode shape
ω	frequency of vibration in Hz
ω_r	natural frequency of r^{th} mode

I. INTRODUCTION

This thesis presents the results of a modal test and analysis of the engineering development unit (EDU) of the NPSAT1 satellite. Furthermore, a finite element model is examined and correlated to the test-results. In addition, we will explore the theory of several parameter extraction techniques.

NPSAT1 is a 82 kg (180 lbs) small satellite hosting a number of experiments. It is a 12-sided cylinder with solar panels mounted on the body. In addition to the top and bottom deck it holds two internal equipment decks. Experiments include two provided by the Naval Research Laboratory, in particular the coherent electromagnetic radio tomography (CERTO) and a Langmuir probe. Other experiments include “a lithium-ion battery, a solar cell measurement system (SMS) experiment, a configurable fault-tolerant processor (CFTP) experiment, two commercial, ‘off-the-shelf’ (COTS)-based experiments, a three-axis micro-electromechanical system (MEMS) rate sensor, and a color digital camera called the visible wavelength imager (VISIM).” [1]. These are NPS-built experiments. For launching NPSAT1 will be attached to the evolved expendable launch vehicle (EELV) secondary payload adapter (ESPA). The modal test will be executed on an engineering development unit (EDU) that replicates the mass distribution of the actual flight unit. Figure 1 shows an exploded view of the flight unit.

After the acquisition of the modal parameters the mode shapes are correlated with the preliminary run finite element model simulation in order to validate it or give suggestions for improvements.

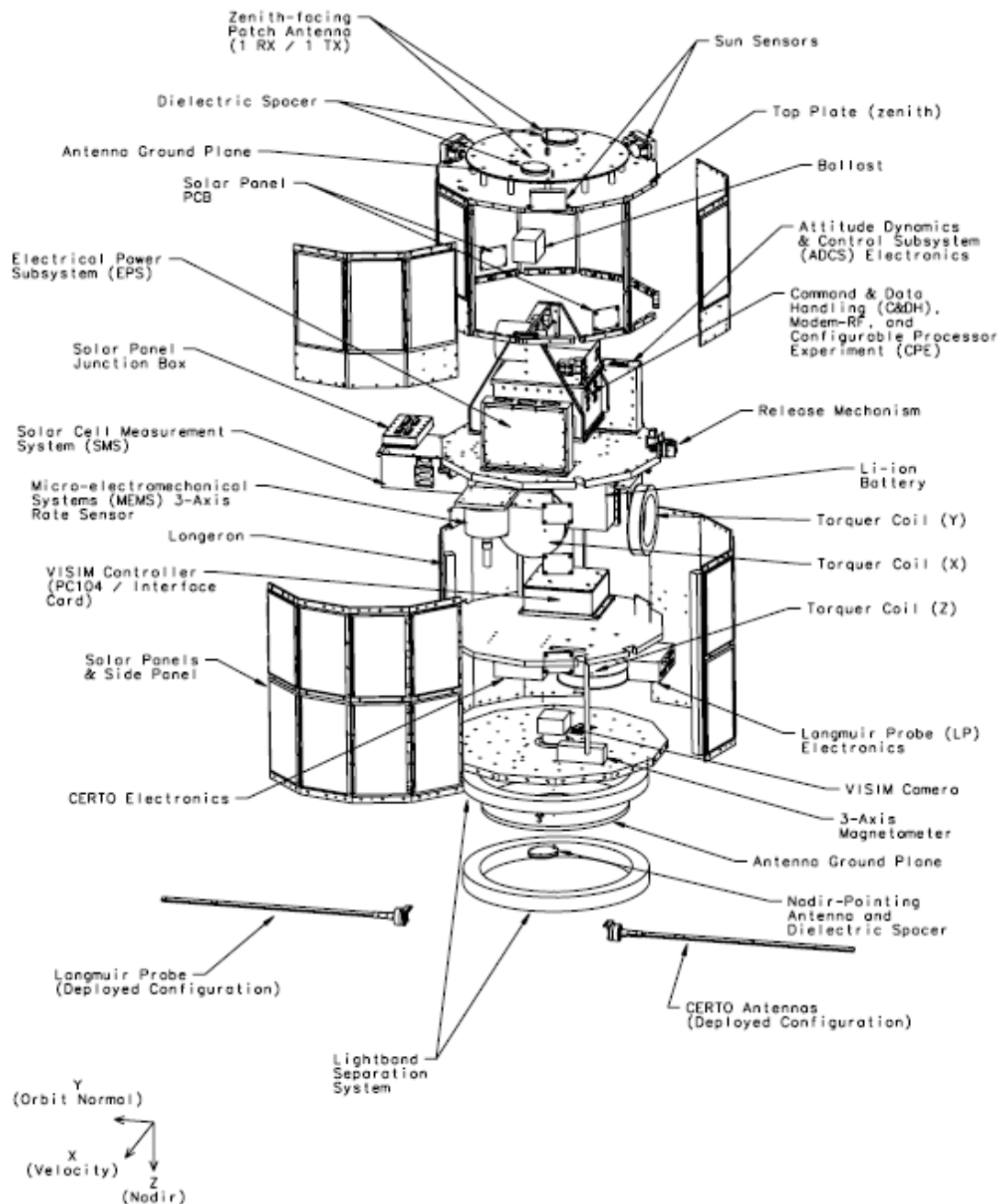


Figure 1: Expanded View of NPSAT1

II. THEORY OF MODAL ANALYSIS

This chapter describes the complex process of analyzing the data acquired from modal testing. We will illuminate several different procedures to extract modal parameters from that data and present some useful tools developed for this purpose. Furthermore, we will examine the role of correlating test results with simulated results more closely. It is understood that this theoretical chapter only accounts for methods used in the experimental section. This chapter does not present a complete theoretical overview of all possible methods used in modal analysis today.

A. BASIC CHECK OF DATA

Although preliminary checking of data represents just a crude procedure, it can be considered a crucial step in modal analysis. The goal of preliminary checking the data is simply to ensure the acquired FRFs are good enough to be analyzed. This prevents wasting time and effort on data that subsequently turns out to be bad data.

1. Low-frequency asymptotes

A simple way to ascertain that the intended boundary conditions have been achieved is to have a close look at the low-frequency behavior of the FRF. Using a log-log plot of the FRF, we take a look at the very low frequencies below the first resonance, because this region correlates to the support conditions chosen for the test.

In case of a grounded structure, we should see a stiffness-like characteristic, which means that the FRF approaches a stiffness line asymptotically at the lowest frequencies. The magnitude should correspond to that of the static stiffness of the structure.

Conversely, in case of a freely supported structure, we should see a mass-like behavior. However, in practice, there will generally be some rigid body modes in case of a freely supported structure, interrupting the mass-like trend.

Deviations from this behavior may stem from data not extending far enough into the lower frequencies or from the intended support conditions not having been achieved necessitating the test-setup to be revised.

2. Mode Indicator Functions (MIFs)

With the increase of automation, mode indicator functions have been developed in order to identify natural frequencies more easily, especially in case of multiple references. In general, test data consist of an $n \times p$ Matrix with n being the number of measurement degrees of freedom (DOFs) and p being the number of excitation or reference DOFs. Usually, n will be a relatively large number and p will be 3 or 4. Overall, the principle behind MIFs is an eigenvalue or singular value decomposition analysis of the FRF-Matrix. A few different MIFs exist and in this chapter the two commonly used will be examined. Different versions of MIF employ different formulations leading either to eigenvalue decomposition or singular value decomposition (SVD). However, both are closely related since the singular values of a rectangular Matrix $[A]$ are the square root of the eigenvalues of a square matrix $[A]^H[A]$.

Possibly, the most widely used MIF is the Complex Mode Indicator Function (CMIF). It is defined as a SVD of the FRF-matrix $[H(\omega)]$ [2]:

$$[H(\omega)]_{n \times p} = [U(\omega)]_{n \times n} [\Sigma(\omega)]_{n \times p} [V(\omega)]_{p \times p}^H \quad (2.1.)$$

$$[CMIF(\omega)]_{p \times p} = [\Sigma(\omega)]_{p \times n}^T [\Sigma(\omega)]_{n \times p} \quad (2.2.)$$

The FRF-matrix is decomposed into a matrix of left singular values $[U]$ and right singular values $[V]$ as well as a rectangular matrix of singular values $[\Sigma]$, all of which are frequency dependent. The mode indicator values are provided by the squares of the singular values and usually plotted on a logarithmic scale. As

Figure 2 shows, natural frequencies are indicated by large values of the first CMIF (peaks), and multiple modes can be detected by use of second and third order CMIF.

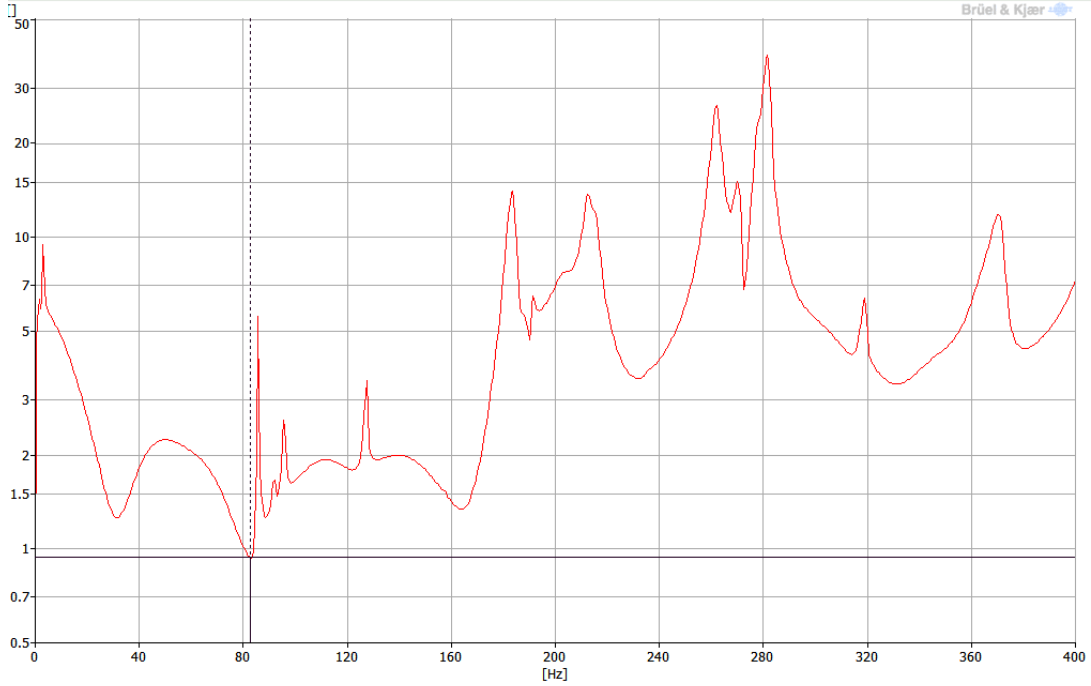


Figure 2: Complex Mode Indicator Function (CMIF)

In case of a multiple mode, the second or even third MIF would show a peak at the same frequency. Additionally, the left singular vector $\{U(\omega_r)\}$ provides an approximation of mode shape for each frequency ω_r and the right singular vector $\{V(\omega_r)\}$ provides an approximation of force patterns.

The other common MIF is the Multivariate Mode Indicator Function (MMIF). This visualization is essentially an eigenvalue decomposition of the FRF-matrix and solves the problem in equation (2.3).

$$\lambda([H]_R^T [H]_R + [H]_I^T [H]_I) \{F\} = [H]_I^T [H]_I \{F\} \quad (2.3)$$

The FRF-matrix has been split up into real $[H_R]$ and imaginary $[H_I]$ parts. The solution to this problem is found by identifying the smallest eigenvalue λ_{min} and corresponding force-eigenvector $\{F_{min}\}$. Plotting the solution results in a

graph similar to Figure 3. It can be observed that the MMIF identifies natural frequencies by minima in the graph.

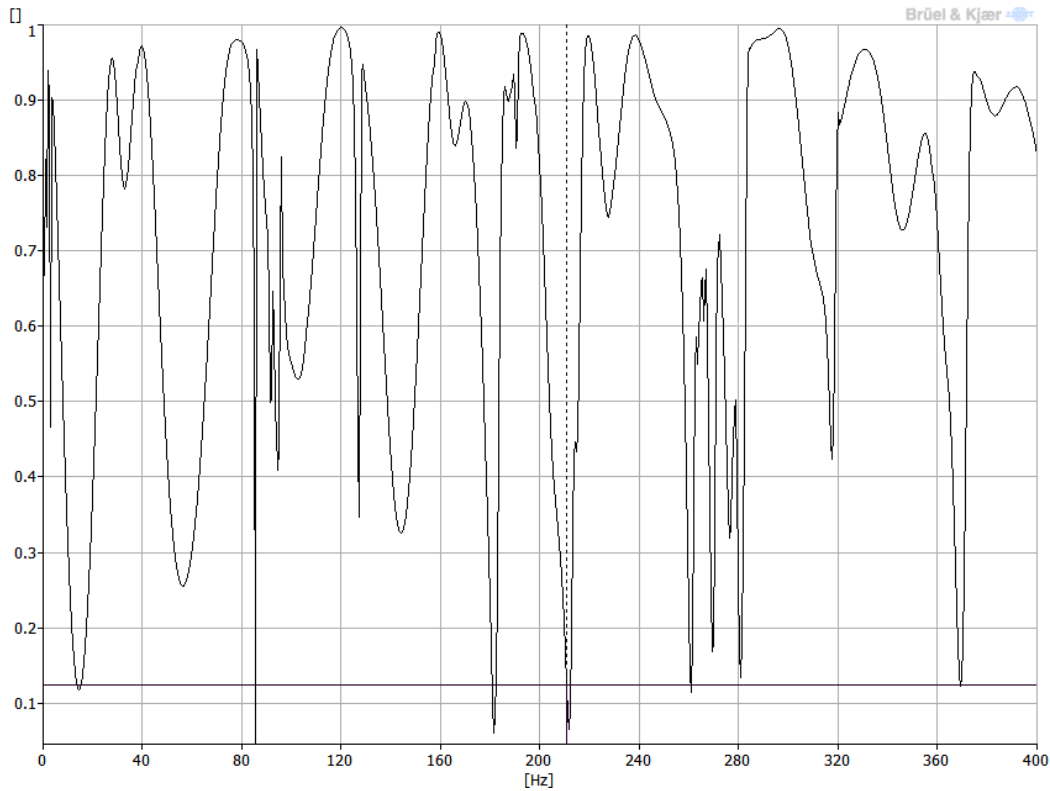


Figure 3: Multivariate Mode Indicator Function (MMIF)

MIFs are very helpful for estimating natural frequencies and validating acquired data. In connection with parameter extraction techniques, described in the next section, they truly become powerful tools.

B. PARAMETER EXTRACTION

One purpose of modal analysis is to extract the modal parameters of a given structure in order to generate the mode shapes and possibly correlating the results to a previously run simulation. Generally speaking, the analyst can choose between single degree of freedom (SDOF) methods and multi degree of freedom (MDOF) methods, however, the test structure more or less dictates which method to use in order to achieve reasonable results. In this section, several SDOF and MDOF methods will be presented and their strength and

weaknesses will be outlined. This serves the purpose to allow better assessment of the results obtained by the modal analysis described in the following chapter.

1. SDOF Modal Analysis Methods

The SDOF-approach has been used since the early days of modal testing. Only in recent times has it been replaced by the more globally working MDOF methods, although even today the SDOF-approach offers some advantages and should not be regarded as outdated. In addition it should be noted that the title of these methods do not refer to the actual degrees of freedom of the tested structure, but rather that only one resonance is considered at a time. Naturally, this implies a limitation of the SDOF methods, the major one being that its accuracy decreases significantly for closely spaced modes. Moreover, this method is quite a time-consuming task and requires a great amount of user interaction. Despite its limitations, this method proved to be valuable especially as a preliminary analysis for quick estimations of the structure's behavior. Ewins even states, "that no large-scale modal test should be permitted to proceed until some preliminary SDOF analyses have been performed" [2].

As we have already seen, SDOF methods rely on the fact that a single mode dominates the behavior of the structure in the vicinity of a resonance. Therefore, after [2], we can simplify the algebraic expression of receptance $\alpha_{jk}(\omega)$:

$$\alpha_{jk}(\omega) = \sum_{s=1}^N \frac{sA_{jk}}{\omega_s^2 - \omega^2 + i\eta_s\omega_s^2} \quad (2.4.)$$

First, it is rewritten as

$$\alpha_{jk}(\omega) = \frac{rA_{jk}}{\omega_r^2 - \omega^2 + i\eta_r\omega_r^2} + \sum_{\substack{s=1 \\ s \neq r}}^N \frac{sA_{jk}}{\omega_s^2 - \omega^2 + i\eta_s\omega_s^2} \quad (2.5.)$$

Now, considering the assumption that in the vicinity of the natural frequency of mode r , the second term becomes independent of frequency ω and thus the sum is simplified to the modal constant ${}_rB_{jk}$. The term for receptance may now be simplified as:

$$\alpha_{jk}(\omega)_{\omega \approx \omega_r} \cong \frac{{}_rA_{jk}}{\omega_r^2 - \omega^2 + i\eta_r\omega_r^2} + {}_rB_{jk} \quad (2.6)$$

This simplification, however, does not diminish the importance of the other existing modes, but rather simplifies their effect to a constant value, which is easier to deal with. In fact, the other modes often do have a significant effect.

a) **Peak-Picking Method**

One of the most straightforward methods is the so-called ‘peak-picking’ method. This method assumes any effect from other modes can be neglected and that the total response is due to the local mode. Naturally, this method works reasonably well for structures that exhibit well-separated modes.

[2] describes the method as follows: The first step in ‘peak-picking’ is to detect the peaks on the FRF plot. One maximum is then taken as natural frequency ω_r of that mode. Next, the corresponding value on the ordinate $|\hat{H}|$ is noted. Following, the ‘half-power points’ are determined as the corresponding frequencies to $\frac{|\hat{H}|}{\sqrt{2}}$, which are referred to as ω_b and ω_a , while $\omega_b < \omega_r < \omega_a$. Subsequently, the damping is estimated from formula (2.7).

$$\eta_r = \frac{\omega_a^2 - \omega_b^2}{2\omega_r^2} = 2\zeta_r \quad (2.7)$$

Last, the modal constant can be determined by

$$A_r = |\hat{H}| \omega_r^2 \eta_r \quad (2.8)$$

It is obvious that this method relies heavily on the accuracy of the maximum FRF level, however, these measurements usually do not provide great accuracy, since most measurement errors occur in the vicinity of a resonance. Furthermore, only real modal constants can be estimated by this method. The other primary limitation is that the single-mode assumption is not strictly correct. Even if the modes are well separated, the neighboring modes have a significant influence on the response of the mode in question.

b) Circle-Fit Method

The circle-fit method uses the Nyquist plot of the frequency response data. For detailed description of the Nyquist plot the reader is referred to chapter 2 in [2]. In summary, the Nyquist plot produces circle-like curves, which ideally, with the appropriate parameters would create an exact circle. Depending on the damping model (viscous or structural) the formulas differ, however the procedure stays the same. In this case the structural model is chosen and thus we will be using the receptance form of FRF.

Since the only effect of the modal constant ${}_r A_{jk}$ is to scale the size of the circle, the basic function for the receptance plot can be used:

$$\alpha = \frac{1}{\omega_r^2 \left[\left(1 - \frac{\omega}{\omega_r} \right)^2 + i \eta_r \right]} \quad (2.9)$$

In the complex plane, equation (2.9) produces a plot shown in Figure 4.

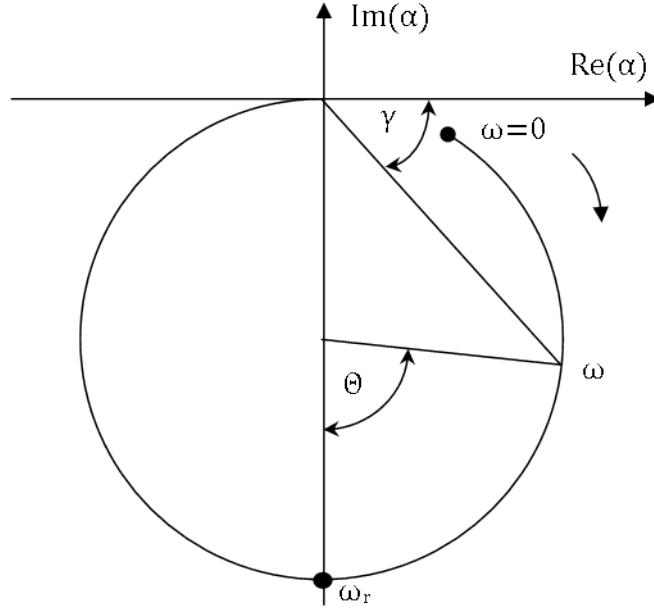


Figure 4: Nyquist plot of FRF

After some algebra, we can obtain the following expression, the reciprocal of which is the rate of sweep of the locus around the circle.

$$\frac{d\omega^2}{d\theta} = \frac{-\omega_r^2 \eta_r \left(1 - \left(\frac{\omega}{\omega_r}\right)^2\right)^2}{2\eta_r^2} \quad (2.10)$$

Equation (2.10) reaches the maximum value when $\omega = \omega_r$, which can be shown by further differentiation. In this case the damping can be calculated using equation (2.10). Another technique to acquire the damping is by using two specific points on the circle ω_b and ω_a , while $\omega_b < \omega_r < \omega_a$. The damping estimates can be obtained from formula (2.11)

$$\eta_r = \frac{\omega_a^2 - \omega_b^2}{\omega_r^2 \left(\tan\left(\frac{\theta_a}{2}\right) + \tan\left(\frac{\theta_b}{2}\right) \right)} \quad (2.11)$$

The procedure itself consists of five steps. During the first step, points are selected for the analysis, either automatically or by the operator. Care should be taken not to choose points that are influenced by other modes and, ideally, the selection should encompass 270° of the circle. Furthermore, the range should not be limited excessively since inaccuracies of the measurements would become more pronounced. In the end [2] recommends to pick at least six points.

The second step consists of finding a circle-fit for the chosen points. This is done by means of least-squares deviation. After the specification of the center and radius, a quality factor is determined, which derives from the mean square deviation of the selected points from the circle. Generally, an error of 1-2% is acceptable.

Now the natural frequency is located in the third step and the correlating damping is obtained. The natural frequency is computed numerically by practically constructing lines from the center of the circle to a succession of points around the resonance curve. The angles between those lines are noted and the rate of sweep is then estimated. From this rate the natural frequency can be identified.

Step 4 is taken to verify and refine the damping estimates. A set of damping estimates is calculated using equation (2.11). Now, either a mean value is computed and taken as the damping for this mode or the values can be examined individually. Ideally, the damping should be the same, however a deviation of 4-5% represents a good analysis. To obtain the modal constant we can now use equation (2.6).

c) *Residual Terms*

Concluding the SDOF-section, it is essential to introduce the concept of residual terms. Since it is usually necessary to limit the range of interest in modal analysis, the residual terms take into account the modes out of range.

When applying the SDOF curve-fit for a series of succeeding modes, a problem usually occurs when working with the extracted parameters. After the

identification of the modes, a construction of a ‘theoretical’ curve that represents these modes is often desired. However, the regenerated curve is usually a bad fit, when compared to actual measurements, and this is due to the effect of out-of-bound modes. Therefore, it is necessary to take modes out of range into consideration.

For a regenerated FRF curve for the modal series from mode m_1 to m_2 we use an equation of the type

$$H_{jk}(\omega) = \sum_{r=m_1}^{m_2} \frac{rA_{jk}}{\omega_r^2 - \omega^2 + i\eta_r\omega_r^2} \quad (2.12)$$

The deviation can be seen clearly, when we look at the equation for the measured data, which accounts for the first mode and the highest mode N , when it is rewritten as equation (2.14).

$$H_{jk}(\omega) = \sum_{r=1}^N \frac{rA_{jk}}{\omega_r^2 - \omega^2 + i\eta_r\omega_r^2} \quad (2.13)$$

$$H_{jk}(\omega) = \sum_{r=1}^{m_1-1} + \sum_{r=m_1}^{m_2} + \sum_{r=m_2+1}^N \left(\frac{rA_{jk}}{\omega_r^2 - \omega^2 + i\eta_r\omega_r^2} \right) \quad (2.14)$$

The first term represents the lower frequencies and approximates to a mass-like behavior. The second term relates to the actual modes in the range of interest, and the third term relates to the higher frequencies, which approximates to a stiffness effect. Thus, equation (2.14) rewrites as

$$H_{jk}(\omega) \cong -\frac{1}{\omega^2 M_{jk}^R} + \sum_{r=m_1}^{m_2} \left(\frac{rA_{jk}}{\omega_r^2 - \omega^2 + i\eta_r\omega_r^2} \right) + \frac{1}{K_{jk}^R} \quad (2.15)$$

where M_{jk}^R and K_{jk}^R are the residual mass and stiffness for that FRF. Naturally, if we extend or limit the range of analysis the residual terms have to be recalculated.

2. MDOF Modal Analysis Methods

As mentioned earlier, there are some situations for which the SDOF assumption is inappropriate. This is the case when the structure is extremely lightly damped or when its modes are closely spaced. The solution is to extract several modes' parameters simultaneously in one process. Naturally, this process is a more complex one and requires an elaborate mathematical understanding. For the detailed mathematical derivation, the reader is referred to chapter 4 of [2]. Before continuing to the two MDOF techniques that shall be discussed, the reader is advised that the idea of residual terms also applies to MDOF methods.

a) *Complex Exponential Method*

The complex exponential method as implemented in NX I-deas, is a MDOF technique that is based on a curve-fitting process in the time-domain. Its main advantage is that it does not rely on estimates of modal parameters as starting points. However, it is limited to the use of only one reference location. For a consideration of multiple references at once, the polyreference method, which evolved from the complex exponential technique, should be employed [3].

In the first step, we obtain the Impulse Response Function (IRF) via an Inverse Fourier Transform of the receptance FRF, which leads to an exponential expression of the IRF:

$$h_{jk}(t) = \sum_{r=1}^{2N} r^{A_{jk}} e^{s_r t} \quad ; \quad s_r = -\omega_r \zeta_r + i\omega_r' \quad (2.16)$$

For simplification purposes, we shall change the following notation:

$$r^{A_{jk}} = A_r \ ; \ e^{s_r \Delta t} = V_r \quad (2.17)$$

Note that since the measured FRF usually a discrete function of equally spaced intervals of frequencies, the IRF also becomes a discrete function of equally spaced time intervals ($\Delta t = 1/\Delta f$). Following this notation, we receive this system of equations for q samples:

$$\begin{aligned} h_0 &= A_1 + A_2 + \dots + A_{2N} \\ h_1 &= V_1 A_1 + V_2 A_2 + \dots + V_{2N} A_{2N} \\ h_2 &= V_1^2 A_1 + V_2^2 A_2 + \dots + V_{2N}^2 A_{2N} \\ &\vdots \\ h_q &= V_1^q A_1 + V_2^q A_2 + \dots + V_{2N}^q A_{2N} \end{aligned} \quad (2.18)$$

Now let the number of samples q exceed $4N$ and we use equation (2.18) to set up an eigenvalue problem, the solution to which will be the complex natural frequencies contained in V_r . In order to obtain this solution we introduce coefficient β_i , which eventually leads to the following polynomial:

$$\beta_0 + \beta_1 V + \beta_2 V^2 + \dots + \beta_q V^q = 0 \quad (2.19)$$

We shall now seek the values of the β coefficients to determine the roots of (2.19) V_1, V_2, \dots, V_q which represent the natural frequencies. In order to do so we let $q \equiv 2N$ and thus the problem

$$\sum_{i=0}^{2N} \beta_i V_r^i = 0 \text{ for } r = 1, \dots, 2N \quad (2.20)$$

results in equation (2.21) to be solved.

$$\{h_0 \quad h_1 \quad h_2 \quad \dots \quad h_{2N-1}\} \begin{Bmatrix} \beta_0 \\ \beta_1 \\ \vdots \end{Bmatrix} = -h_{2N} \quad (2.21)$$

This process is repeated with a different set of IRF data, always overlapping for all but one. Thus, the second problem would look like:

$$\{h_1 \quad h_2 \quad h_3 \quad \dots \quad h_{2N}\} \begin{Bmatrix} \beta_0 \\ \beta_1 \\ \vdots \end{Bmatrix} = -h_{2N+1} \quad (2.22)$$

Eventually, this results in a set of $2N$ linear equations, which can then be solved for β :

$$\{\beta\} = -[h]^{-1}\{\tilde{h}\} \quad (2.23)$$

After having obtained the coefficient β we can now determine the values V_1, V_2, \dots, V_{2N} (2.19) and thus are able to determine the natural frequencies using (2.17). Furthermore, we may determine the modal constants using equation (2.24).

$$[V]\{A\} = \{h\} \quad (2.24)$$

The complex exponential method is used in the following manner. First, an estimate for the number of degrees of freedom is made and based upon this the analysis mentioned above is performed. Subsequently, the extracted modal parameters are used to create a regenerated FRF, which in turn is compared to the original measurements. Now, the error between the artificial and the real curve is computed. This process is then repeated several times, each time using a different initial estimate of the degrees of freedom. Eventually, as the estimate of the DOFs approaches the value of the actual DOFs, the error should diminish. Thus, the modal parameters can be plotted in a so-called stability diagram as Figure 5 shows. If the initial DOFs estimate is higher than the actual DOFs, computational modes are created. Generally, they can be identified by their

unusually high damping or small modal constants. The stability diagram plots the results of each iteration (right-hand side axis) and assigns different symbols for different kind of stabilization:

- stable mode (red diamond)
- vector stable (blue triangle)
- frequency stable (green X)
- damping stable (pink asterisk)
- new mode (cyan cross)
- computational mode (usually filtered, because undesirable)

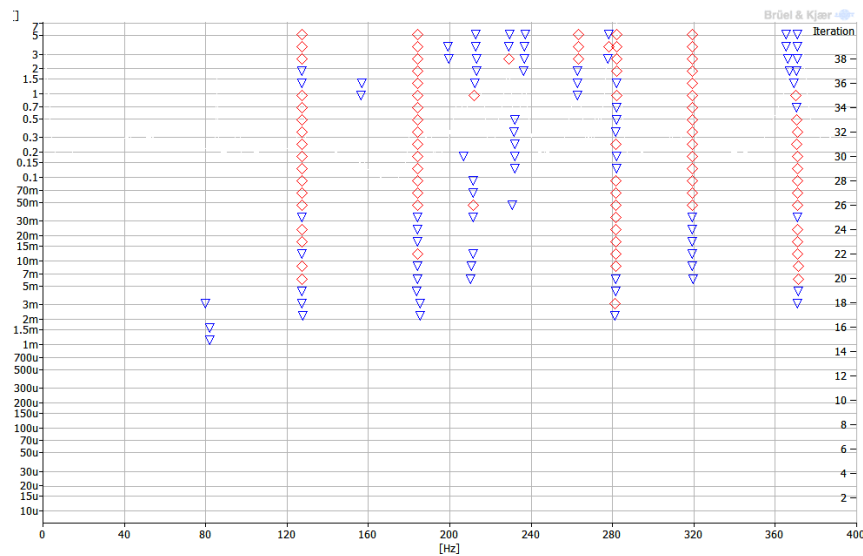


Figure 5: Example of Stability Diagram

b) *Rational Fraction Polynomial Method*

The most widely used MDOF frequency domain method is the rational fraction polynomial method (RFP). It is an advancement of the non-linear least-squares method and in contrast to its parent, method uses a rational fraction FRF expression. The advantage the RFP method has over its predecessor is, that the curve-fitting problem can be formulated as a set of linear equations and thus allows for a matrix solution.

Theoretically, this set of linear equations allows for the solution of every unknown parameter. However, the RFP method presumes the order of the mode to be known, when it usually is not and is one of the parameters that are to be extracted. Therefore, an iteration process is implemented using different values for the mode order and comparing the results. This leads to the calculation of genuine modes as well as so called computational or fictional modes. In principle a mode that repeats after several iterations and is persistent, is most likely a genuine mode. Modes that vary excessively and occur sporadically throughout the iteration process are most likely computational modes. Usually, the results of the iteration process are plotted in a stability diagram (Figure 5) and the analyst can choose the modes that appear to be the best fit. Modern analysis software also provides an automatic selection feature. It is at this point, that the MIF come into action as a powerful tool. In order to help the operator with his/her selection, the stability diagram can be overlaid with a MIF, so that the modes can be identified more easily (Figure 6).

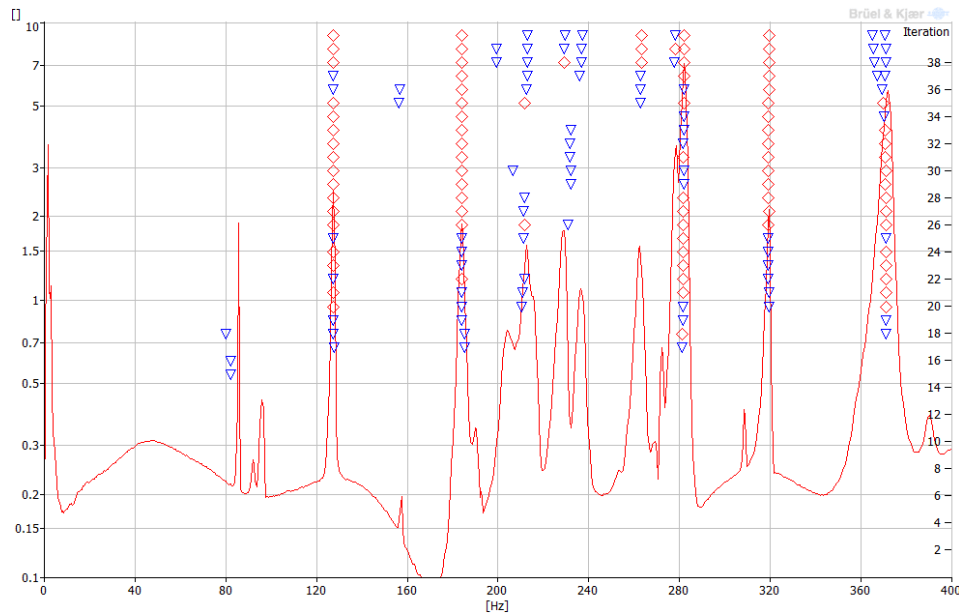


Figure 6: Example of Stability Diagram MIF Overlay

This advanced technique also allows to choose between global solution and local solution. Essentially, the local solution is advisable for non-consistent

data, which may be caused due to mass-loading. In general, for a complex structure one may have an inadequate number of accelerometers and is required to do several measuring cycles during which the accelerometers are moved, while the force input remains the same. Thus, every desired node is measured in one set of data. However, the change of mass-distribution will cause discrepancies in the different cycles' data, resulting in a shift of resonance frequency. Figure 7 illustrates this effect. Clearly, the resonance appears to be in a range of frequencies, rather than a single one. The local solution feature allows for compensation of this effect by calculating a mean value in a specified range. This mean value is then used for the parameter extraction algorithm.

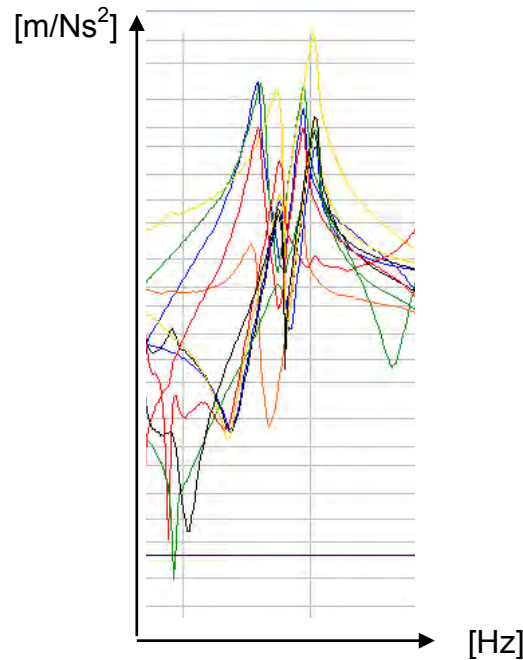


Figure 7: Example of Frequency Shift

C. CORRELATING TEST RESULTS AND SIMULATION RESULTS

In this section, two slightly different concepts shall be discussed. First, the frequency response assurance criterion (FRAC) is explained, followed by the introduction of the modal assurance criterion (MAC).

1. Frequency Response Assurance Criterion

The frequency response assurance criterion compares two frequency response functions and assigns a value between zero and one, with one representing complete correlation. It is often used for methods with high user interaction such RFP where the user has to choose a mode on the stability diagram. In this case, FRAC can be used to correlate the regenerated FRF with measurement FRF in order to determine whether the parameters extracted represent a good fit. Ideally, the synthesized and measured FRF should be linearly related. Furthermore, this feature can be used in any case for validation of the parameter estimation method. [4] gives the equation this technique uses to calculate an assurance value:

$$FRAC_{pq} = \frac{\left| \sum_{\omega=\omega_1}^{\omega_2} H_{pq}(\omega) H_{pq}^*(\omega) \right|^2}{\sum_{\omega=\omega_1}^{\omega_2} (H_{pq}(\omega) H_{pq}^*(\omega)) \sum_{\omega=\omega_1}^{\omega_2} (H_{pq}(\omega) \hat{H}_{pq}^*(\omega))} \quad (2.25)$$

2. Modal Assurance Criterion

After the analysis of the experimentally obtained data, the results can be used to validate a finite element model. For that purpose the modal assurance criterion has been developed. Although the mode shapes of the simulation and the shapes of the experiment may differ by number, they can still represent the same mode, and thus validate the simulation. For further details on MAC, the reader is referred to [3] and [4].

The modal assurance criterion is a scalar value that can range between zero and one, with a value close to zero representing low correlation and a value

near to one indicating a high correlation. The latter case means that the two mode shapes represent the same motion but differ by a complex modal scale factor (MSF). Let m be the total number of modes identified in the bandwidth of interest, then the MSF is determined by

$$MSF = \frac{\{\psi_1\}^H \{\psi_2\}}{\{\psi_1\}^H \{\psi_1\}} \quad (2.26)$$

With ψ_1 being an m -dimensional vector representing mode shape 1 and ψ_2 being an m -dimensional vector representing mode shape 2. In this notation mode shape 1 is the reference shape to which shape 2 is compared.

The modal assurance criterion is calculated using the expression

$$MAC = \frac{|\sum_{j=1}^m \{\psi_1(j)\}^* \{\psi_2(j)\}|^2}{\sum_{j=1}^m (\{\psi_1(j)\}^* \{\psi_1(j)\}) \sum_{j=1}^m (\{\psi_2(j)\}^* \{\psi_2(j)\})} \quad (2.27)$$

There are five reasons why the MAC may take a value near zero:

- the system is non-stationary because of changes of mass, stiffness and damping during testing
- the system is non-linear
- there is noise in the reference mode shape
- the chosen parameter extraction technique is invalid
- the mode shapes are linearly independent

If the first four reasons can be eliminated MAC can be used for an orthogonality check. Although it does not consider mass or stiffness matrices, MAC can provide an approximation for orthogonality.

The MAC takes a value close to one if:

- the number of DOFs is insufficient to distinguish independent mode shapes
- unmeasured forces to the system influence mode shapes
- the mode shapes consist of coherent noise

- the shapes represent the same motion differing only by modal scalar factor

If the first three reasons can be eliminated MAC can be used to identify correlating mode shapes. There are different ways to display the information MAC provides. In its simplest form a table is created arranging each mode of the simulation against each mode of the experimental analysis. Ideally, the diagonal would show values of one, while the other fields would be zero. An example is given in Table 1. This concept can also be displayed visually, either in a 2D or 3D plot. Different colors represent different values of MAC, as can be seen in Figure 8.

[Hz]	137.885	214.971	353.328	374.926	474.509	494.683
135.567	0.166	0.017	0.003	0.001	0.007	0.161
146.986	0.753	0.001	0.006	0.044	0.192	0.006
210.486	0.008	0.921	0.005	0.028	0.002	0.024
337.545	0.002	0.048	0.745	0.658	0.001	0.004
374.909	0.001	0.000	0.146	0.127	0.027	0.008
492.755	0.167	0.005	0.020	0.002	0.793	0.003
512.627	0.068	0.011	0.008	0.004	0.010	0.767

Table 1: Example of Numerical Presentation of MAC

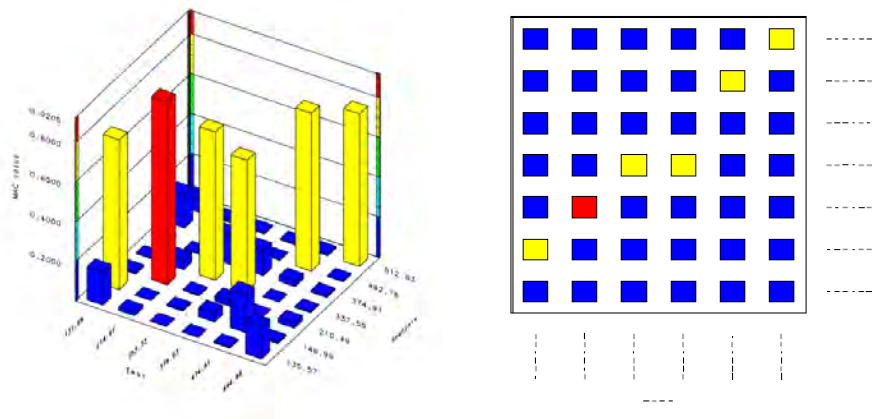


Figure 8: Example of 3D and 2D Presentation of MAC

THIS PAGE INTENTIONALLY LEFT BLANK

III. MODAL TESTING OF NPSAT1

This chapter describes the process of the modal survey of NPSAT1. First we will examine the test-setup and the reasons for the properties chosen. Following a brief outline of the test process itself, emphasis will be placed on a more detailed description of the analysis process.

A. TEST SETUP

The purpose of this thesis is to validate a preliminary run of a finite element model of NPSAT1. There are some requirements associated with this task. For further detail on the implications of the choices made in the following the reader is referred to the preceding Studienarbeit [5].

First, the boundary conditions under which the structure is to be tested are already determined by the FEM. In this case the choice was made for a freely supported structure. A framework and rubber cords allow for this condition. Furthermore, the three-dimensional structure demands three degrees of freedom being measured at each node. Additionally, the locations of the transducers have to be chosen and their coordinates implemented into the computer model. Since there are only 8 tri-axial transducers available, but 168 nodes to be measured, the testing has to be split into several sessions. Because of this and the associated repositioning of the accelerometers, the choice is made to use wax as an adhesive with the obvious advantage, that the transducers can be loosened easily. In addition, impact excitation via hammer is chosen because it offers the most efficient test setup. Using a shaker, for instance, would require a much more complex setup in order to support the 82 kg satellite structure. Furthermore three different locations of excitation are chosen (nodes 123, 159, 169) each in a different direction resulting in the structure being excited in all three dimensions. Thus we can assume to excite every mode in the bandwidth of interest. The final test setup is shown in Figure 9 as well as the computer model.

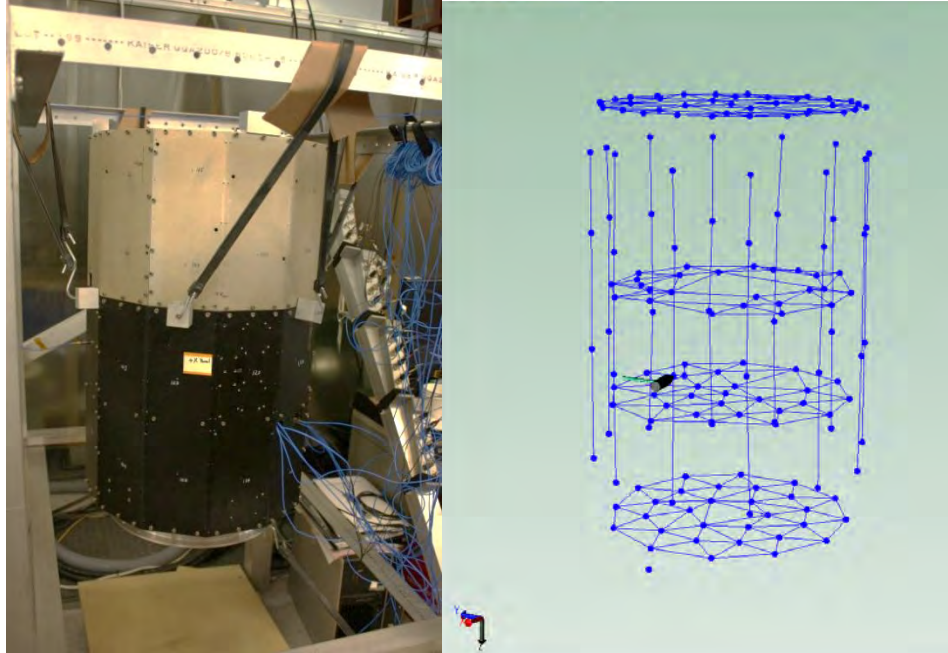


Figure 9: Test Setup Free Boundary Conditions and Computer Model

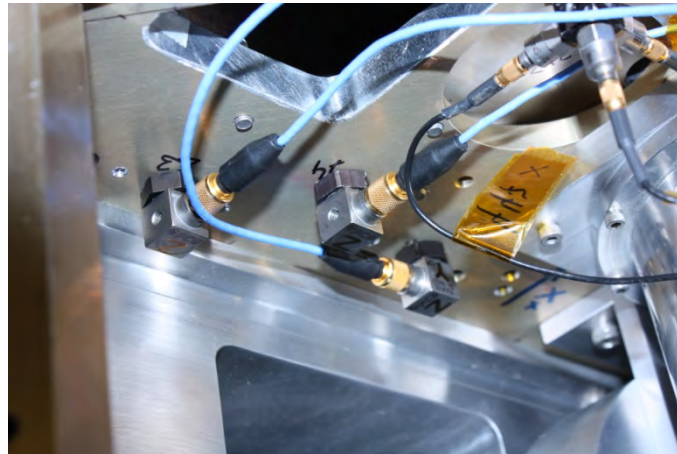


Figure 10: Fixed Accelerometers

B. MEASUREMENTS

During the acquisition of data, the operator has to consider several important aspects. First of all, the bandwidth of interest is determined. Since the lower frequencies represent the highest mass participation, a range from 0 - 400 Hz is chosen. Another key factor is the adjustment of the sensitivity of the accelerometers. It is essential not to cause an overload because this leads to

loss of information. However, it is not advisable to have too low a sensitivity because that introduces noise into the data. Therefore, before starting a measurement cycle, the sensitivity should be adjusted. In addition, the use of wax as an adhesive may cause the accelerometers to loosen during data acquisition. Especially for the measurements taken inside the satellite, this may not be obvious during the data acquisition. Thus, it is necessary to carefully check if the accelerometers are still attached after the measurement cycle. It is advisable to do a preliminary data check after each data acquisition in order to detect any abnormalities. This possibly saves time during the analysis process if any cycle has to be repeated or the desired boundary conditions have not been achieved.

C. MODAL ANALYSIS

During this section we will analyze the obtained data according to the different methods mentioned in chapter 2. We will follow the path from the easy and crude SDOF techniques to the more sophisticated MDOF methods. During the analysis two programs were used. For the SDOF-analysis as well as for the acquisition of data, the software 'NX I-deas' developed by Siemens was used. For the MDOF-analysis as well as the correlation tasks, 'PulseReflex' developed by Brüel & Kjær was used.

1. Peak-Picking Method on NPSAT1 Data

For initial parameter estimation, we will use the peak-picking method in order to get an estimate of the modes present. This method represents a fairly simple technique requiring minimal operator interaction. However, some limitations may apply because of the rather complex structure.

The first step is to pick the peaks on an FRF graph. During this analysis, we will emphasize the structural damping and thus use FRF data from the responses. When viewing the FRF it is already apparent, that the SDOF-assumption is not fully valid, because of the closely spaced peaks around the 90

Hz and 260 Hz area (Figure 11). Furthermore, the range for the analysis is set to 70 Hz – 400 Hz, because of the noise and rigid body modes that appear in the lower range.

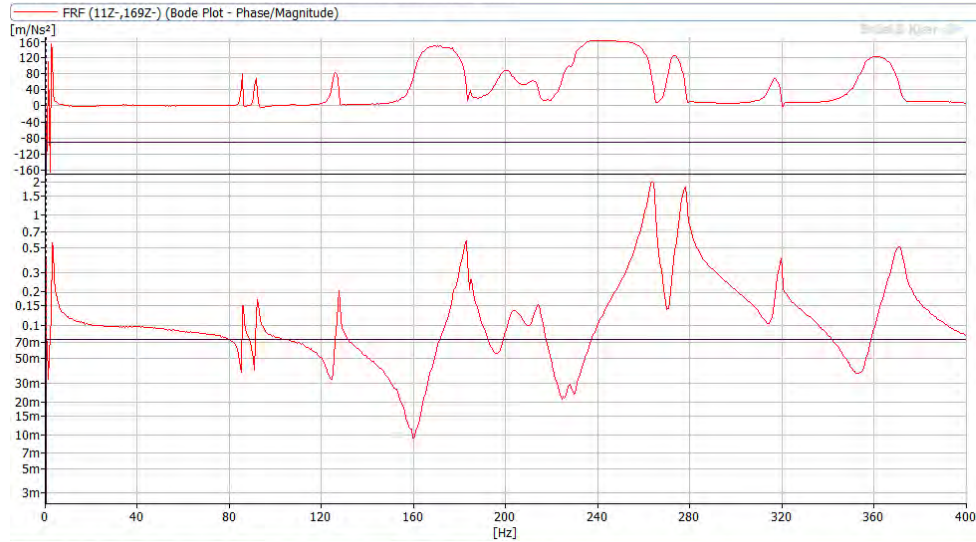


Figure 11: FRF Ref: 123X-; Res: 11X+

After having chosen the frequencies of the peaks, I-deas calculates a curve-fit. It is also advisable to include residual terms on both ends to compensate for the influence of out-of-band modes. Comparing the curve-fit suggestions to the original data, it is obvious that this method does not provide an accurate estimate for the modal parameters. However, we obtained up to eleven modes using the Z-direction of excitation and we provide an estimate of the number of modes to look for using methods that are more sophisticated. Table 2 shows the results obtained with the peak-pick technique for all three directions of excitation. Note, that the modes found are already correlated to the final mode count, thus it can be seen which modes failed to be detected by this method.

Mode	SDOF PeakPick X		SDOF PeakPick Y		SDOF PeakPick Z	
	f [Hz]	d [%]	f [Hz]	d [%]	f [Hz]	d [%]
1	84.802	0.087	83.473	0.126	82.688	0.152
2	92.882	0.009	96.336	0.512	92.464	0.176
3			127.722	0.181	127.460	0.252
4	184.659	0.013			183.594	1.251
5					183.920	0.661
6					204.179	1.615
7					212.894	0.381
8	228.096	0.504	228.371	0.416		
9	235.336	0.248	236.104	0.266		
10	264.948	0.009	262.708	0.101	265.755	0.671
11	289.624	0.251	278.168	0.244	277.711	0.410
12			320.008	0.039	319.179	0.154
13					369.360	0.286
14	373.363	0.004	372.541	0.268		

Table 2: Mode Table Using Peak-Picking Method

2. Circle Fit Analysis of NPSAT1

First, the operator chooses a response FRF from the measured data, which appears to represent the modes rather clearly. Afterwards, the first frequency peak is picked with the peak-picking tool. Now, the residual terms and the single curve fit are calculated. For the calculation of the curve-fit, a Nyquist plot is used (similar to Figure 12) and the tolerance settings can be adjusted, to achieve a high correlation. As mentioned in the previous chapter, a correlation of 98% provides a very good curve-fit, as long as at least six points are used.

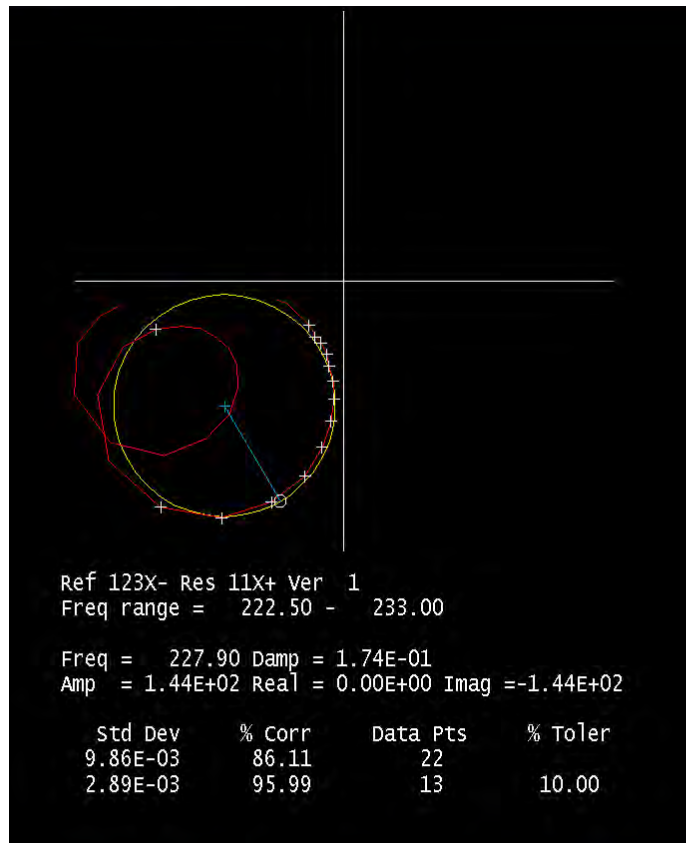


Figure 12: Circle Fit Nyquist Plot Response 11X+ Reference 123X-

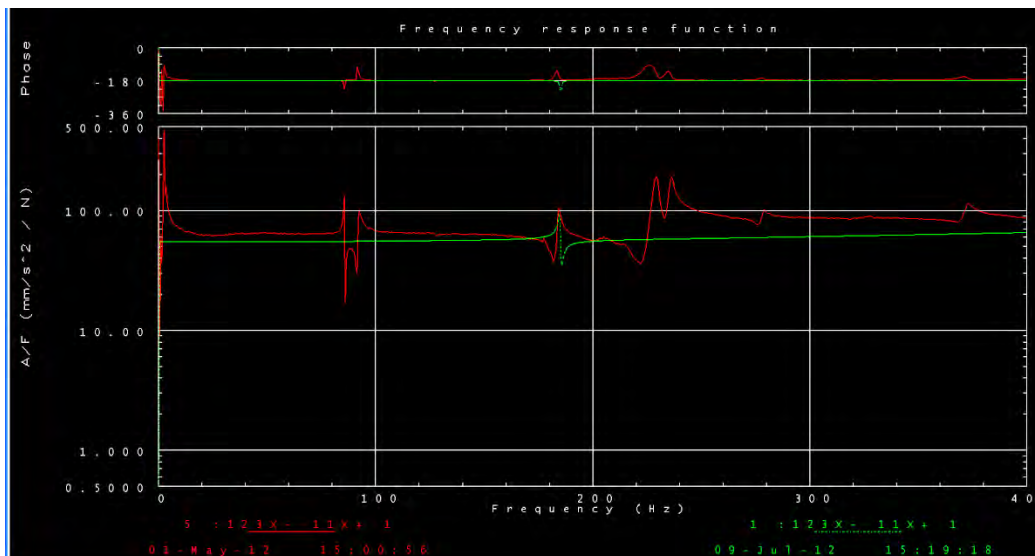


Figure 13: Circle Fit Single Mode Curve Fit

The result is a curve-fit for a single mode (Figure 13) which can be adjusted further if needed. From this curve-fit the software calculates the mode shapes for each response point, resulting in a 3D animation (Figure 14) of the local movements. The analyst now proceeds to the next mode and repeats this process. In the end, this process was repeated for all three references and the results are listed in Table 3.

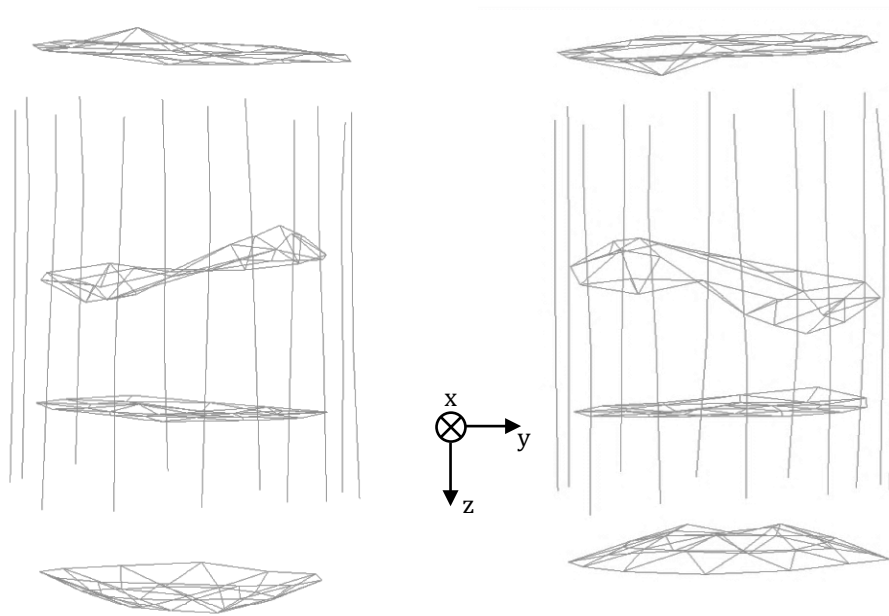


Figure 14: 3D Animation of Mode 14 Using Circle Fit Method

Mode	CircleFit X		CircleFit Y		CircleFit Z	
	f [Hz]	d [%]	f [Hz]	d [%]	f [Hz]	d [%]
1	83.558	0.026	84.527	0.019	86.216	0.246
2	92.970	0.805	94.271	0.689	90.246	0.609
3					122.140	1.020
4	184.712	0.327	185.116	0.187	180.012	1.389
5			204.020	1.470	202.143	1.911
6					213.821	0.522
7	227.786	0.433	229.006	0.116		
8	233.787	0.722	233.811	0.900		
9					261.742	0.620
10						
11					277.457	1.143
12			319.740	0.443	314.065	1.203
13						
14	383.873	0.303	373.322	0.057	368.994	1.333

Table 3: Circle-Fit Results

3. Complex Exponential Analysis of NPSAT1 in Frequency Domain

After having gained an overview of possible modes, we can now try to achieve the best curve-fit and thus the most accurate modal parameters. Therefore, MDOF techniques represent a more promising approach.

The first step using the complex exponential method is to calculate the MIF for one set of data. Then, the algorithm can be refined choosing different options. One very important option is the number of iterations to be used calculating the stability diagram. In this case, a number of 50 iterations seems sufficient to distinguish the modes.

As a result, a stability diagram is provided, overlaid with the complex mode indicator function and one measurement FRF for visual assurance. Figure 15 shows the stability diagram for the Z-reference. The circles represent the

modes picked by the operator. The operator chooses the points according to their influence on the curve-fit and their stabilization. This means that stable modes are preferred (indicated by a red diamond).

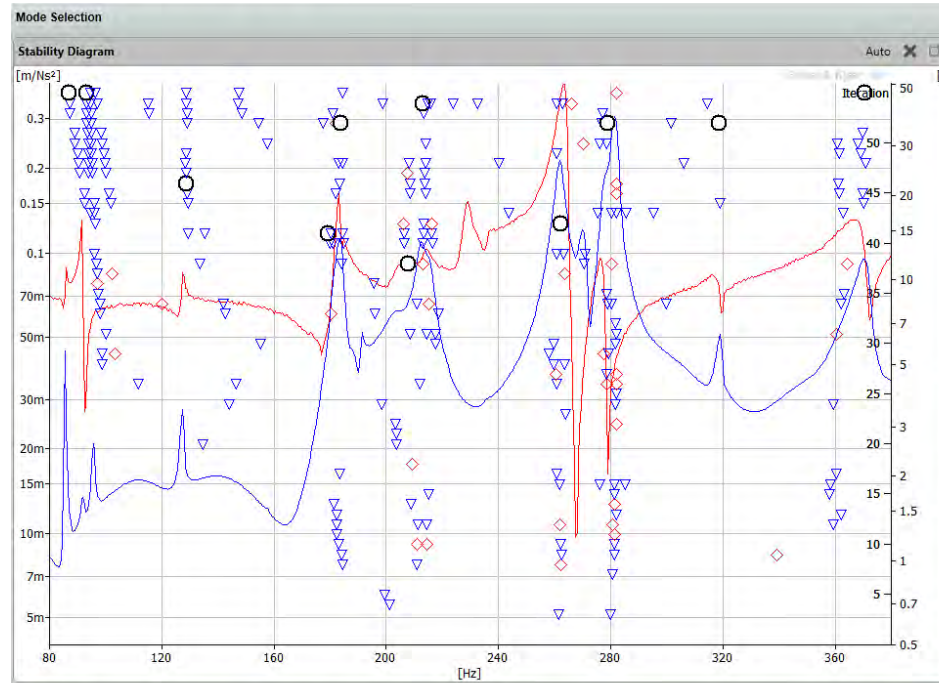


Figure 15: Complex Exponential Mode Selection Z-Reference

Furthermore, the operator constantly watches the FRAC value for the measurement FRF and regenerated FRF in order to achieve the highest value possible. Using the complex exponential technique, FRAC values up to 92% can be achieved. However, FRAC values as low as 20% still exist. The extracted mode parameters are shown in Table 4.

Mode	PolyRef Freq X		PolyRef Freq Y		PolyRef Freq Z	
	f [Hz]	d [%]	f [Hz]	d [%]	f [Hz]	d [%]
1	85.813	0.058	86.185	0.031	86.917	0.011
2	95.449	0.214	93.983	0.219	93.100	0.061
3	120.919	1.779	127.825	0.302	128.938	0.258
4	184.163	0.595	185.624	0.271	179.375	1.388
5					183.950	0.181
6	203.764	2.317	205.561	3.641	207.777	2.342
7	214.232	0.466	214.887	0.405	213.181	0.937
8	228.200	0.795	229.378	0.870		
9	237.687	0.256	235.346	0.954		
10	262.839	0.300	262.652	0.502	262.087	0.700
11	276.964	0.417	277.941	0.610	279.128	0.677
12			282.654	0.313	318.550	0.276
13			319.188	0.243		
14	372.550	1.002	371.080	0.760	370.635	0.204

Table 4: Modal Parameters Using Complex Exponential Technique

4. Rational Fraction Polynomial Analysis of NPSAT1

In the end, we will use the most sophisticated method available for modal analysis, the rational fraction polynomial method. First, we will use the global solution, after which we will move on to the local solution to reduce data inconsistencies.

The operator's procedure using the RFP method is very similar to the complex exponential method. First, the CMIF is calculated and the options of the algorithm are set. In this case we require 55 iterations to identify the lowest mode around 85 Hz. Following the settings, the stability diagram is calculated and the operator can start the curve-fitting process. An example of the stability diagram is shown in Figure 16. The modes identified using the RFP global method allow for a FRAC value of up to 95%. Furthermore, the lowest FRAC values are lifted to around 30%. Thus, we achieved an improvement of accuracy. Table 5 shows the results of the rational fraction global solution.

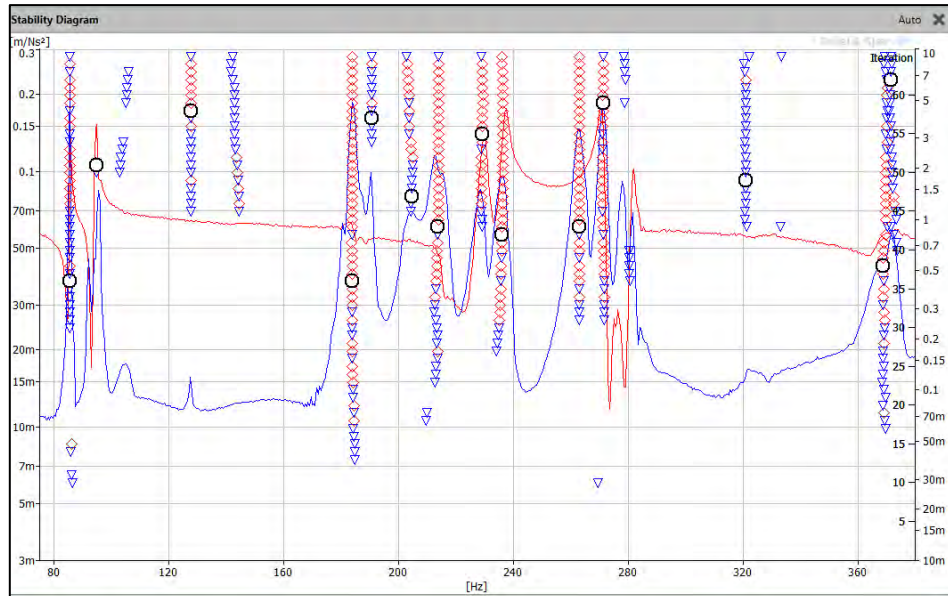


Figure 16: Stability Diagram RFP Global X-Reference

Mode	RFP glob X		RFP glob Y		RFP glob Z	
	f [Hz]	d [%]	f [Hz]	d [%]	f [Hz]	d [%]
1	85.482	0.158	85.610	0.085	85.843	0.051
2	94.767	0.001	95.465	0.105	95.113	0.509
3	127.697	0.330	127.372	0.627	127.064	0.424
4	183.894	0.509	184.161	0.750	182.151	0.991
5	190.631	0.137				
6	204.541	0.823	202.224	1.494	201.492	0.969
7	213.809	0.832	213.728	0.502	212.551	1.255
8	229.179	0.538	229.337	0.755	231.372	0.841
9	236.096	0.520	236.922	0.525	261.568	0.707
10	263.025	0.478	263.035	0.416	267.525	0.254
11	271.276	0.293	282.032	0.318	280.761	0.285
12	321.021	0.209	319.263	0.217	318.124	0.310
13	368.888	1.458				
14	371.472	0.465	370.760	0.768	369.992	0.518

Table 5: Mode Table using RFP Global Solution

However, when scrutinizing the data, it is apparent that frequency shifts occur during the different measurement cycles. This is most likely caused by

mass loading effects. Mass loading occurs when the accelerometers are moved during the measurement cycles. This results in a slightly different mass distribution and thus results in a frequency shift of the resonance.

The local solution offers compensation for this effect. Essentially, the algorithm calculates the modes for each measured FRF and plots it in a cluster diagram, which is again overlaid with the MIF for visual aid (Figure 17). The operator can now use an 'area'-tool to envelop a selection of modes and calculate the midpoint of that cluster. The extracted parameters are thus a compromise of all available modes. Furthermore, obvious measurement errors can be left out so they do not influence the result. This method proves to be the most accurate, as it finds the highest number of modes and allows for a FRAC value of up to 99%. The average FRAC value is 83.6%. The results are given in Table 6.

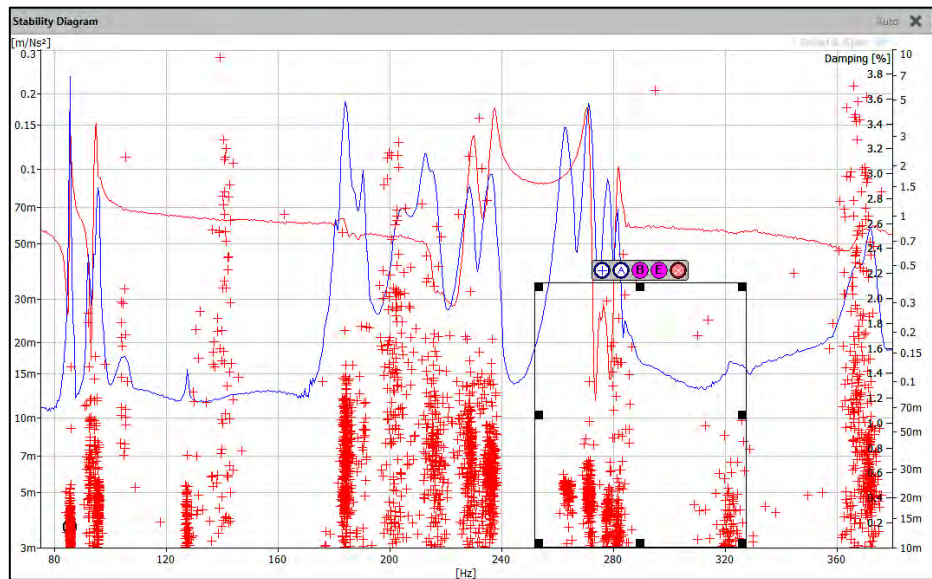


Figure 17: Cluster Diagram RFP Local X-Reference

Mode	RFP loc X		RFP loc Y		RFP loc Z	
	f [Hz]	d [%]	f [Hz]	d [%]	f [Hz]	d [%]
1	85.601	0.165	85.668	0.207	85.365	0.256
2	94.726	0.460	95.242	0.370	93.991	0.376
3	127.466	0.266	127.153	0.496	127.074	0.679
4	184.119	0.669	183.926	0.638	182.948	1.022
5	190.219	0.805	202.852	1.192	203.248	1.705
6	202.551	1.298	216.139	0.754	215.073	0.906
7	216.054	0.747	229.211	0.707	228.777	0.636
8	228.635	0.714	236.354	0.483	235.075	0.540
9	235.898	0.604	263.923	0.440		
10	263.154	0.457	271.276	0.363	268.313	0.758
11	271.251	0.404	281.032	0.370	279.633	0.443
12	280.381	0.259	318.567	0.246	317.706	0.384
13	321.790	0.260	360.341	1.245	362.943	1.118
14	369.463	1.054	371.804	0.814	370.116	0.787

Table 6: Mode Table Using RFP Local Solution

THIS PAGE INTENTIONALLY LEFT BLANK

IV. CONCLUSION AND OUTLOOK

The preliminary check of the acquired data offered first validation of the test-setup. All acquired FRFs have a clear mass-like behavior in the low frequencies only interrupted by the rigid body modes. Therefore, the desired boundary conditions have been achieved. However, the high frequency asymptotes of the point mobility measurements of both the X and Y direction show a stiffness-like behavior (Figure 18). This fact makes it rather difficult for the analyst because the modal parameters are dominated by the local effects. Figure 18 clearly demonstrates the difficulty in identifying the modes. Usually, it is advisable in such a case to change the location of excitation, however relocation to another point on the outside panels does not promise to achieve any improvement.

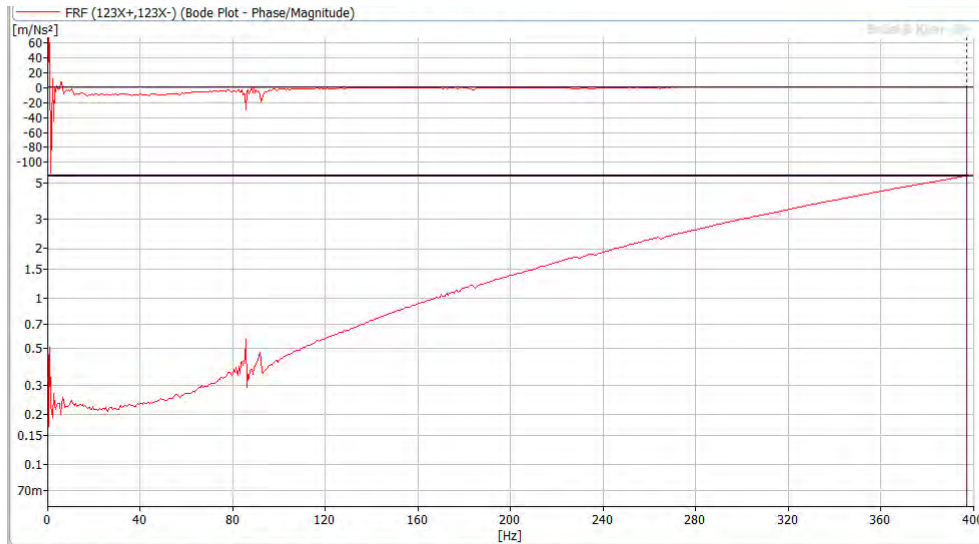


Figure 18: Point Mobility FRF Ref: 123X-

During the analysis process, it became apparent that the SDOF-assumption is not applicable in this instance. However, the results obtained with the SDOF methods provided a good estimate of the resonance frequencies and helped identify the modes when applying more sophisticated techniques.

One aspect that the SDOF methods display better than the MDOF methods is the influence of excitation on the different mode shapes. Especially

the circle fit method showed that certain mode shapes are excited better in one direction than the other.

Since the RFP local solution in X direction offers the best curve-fit, it is chosen to correlate to the FEM results in order to validate the model. For this task a MAC graph is calculated (Figure 19). As can be seen in the graph the mode shapes correlate very badly. Moreover, the first mode calculated by the FEM simulation is located at 200.674 Hz which is significantly higher than the first mode identified by modal testing (85.601 Hz; RFP local X).

Simulation

	200.674	226.231	303.423	455.542	459.007	487.521	488.341	524.024	548.658	631.798	754.151	782.048	787.789	788.031
RFP local X-Reference														
85.601	0.003	0.000	0.002	0.001	0.000	0.001	0.003	0.049	0.024	0.002	0.000	0.001	0.000	0.019
94.726	0.068	0.003	0.001	0.002	0.001	0.005	0.004	0.001	0.011	0.001	0.001	0.002	0.000	0.013
127.466	0.130	0.049	0.006	0.003	0.011	0.021	0.032	0.000	0.008	0.006	0.012	0.001	0.000	0.001
184.118	0.718	0.181	0.033	0.005	0.018	0.027	0.009	0.007	0.001	0.002	0.000	0.000	0.001	0.000
190.219	0.555	0.601	0.047	0.001	0.002	0.023	0.037	0.001	0.004	0.008	0.000	0.003	0.001	0.001
202.552	0.147	0.462	0.020	0.014	0.011	0.011	0.014	0.004	0.002	0.003	0.004	0.007	0.000	0.000
216.054	0.450	0.637	0.010	0.004	0.002	0.015	0.053	0.000	0.008	0.002	0.003	0.005	0.000	0.000
228.634	0.001	0.010	0.003	0.001	0.000	0.027	0.001	0.100	0.002	0.000	0.000	0.000	0.000	0.002
235.898	0.032	0.043	0.112	0.000	0.001	0.045	0.000	0.040	0.001	0.000	0.000	0.001	0.000	0.001
263.155	0.006	0.004	0.414	0.001	0.099	0.001	0.000	0.009	0.186	0.004	0.000	0.000	0.000	0.000
271.251	0.067	0.012	0.314	0.000	0.011	0.020	0.001	0.011	0.121	0.001	0.000	0.005	0.000	0.000
280.380	0.009	0.007	0.315	0.002	0.170	0.026	0.001	0.002	0.035	0.005	0.000	0.000	0.000	0.000
321.791	0.027	0.009	0.020	0.002	0.004	0.013	0.016	0.001	0.000	0.007	0.008	0.001	0.000	0.001
369.462	0.001	0.005	0.001	0.000	0.016	0.117	0.000	0.039	0.003	0.001	0.000	0.002	0.000	0.002

Figure 19: MAC Simulation vs. RFP local X-Reference

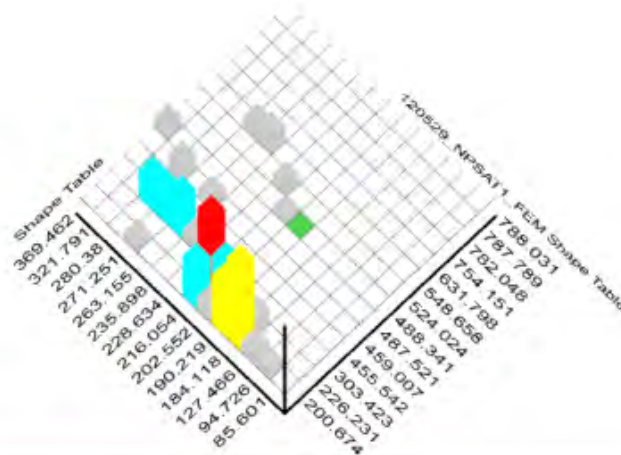


Figure 20: 3D MAC Simulation vs. RFP local X-Reference

Therefore, the FEM is considerably stiffer than the actual structure. This results from the connections in the model which represent a welded connection rather than a connection by screws. As a result, the FEM has to be modified by considering the connection conditions of each part. The model has to be more flexible for it to reproduce the actual structure of NPSAT1.

In order to validate the test results, each mode table is correlated to the RFP local X-Reference table. Thus, we can determine if the acquired results are consistent. First, it is obvious that even the SDOF-methods identify modes that are in the same range as the modes found by the other techniques. Furthermore, when correlating the results of the MDOF techniques with the RFP local X Reference, a clear diagonal trend is apparent. Thus, we can assume that the test results are in fact valid.

In conclusion, the test results appear to be genuine and the test-setup provides the demanded boundary conditions. The correlation with the finite element model, however, proves to be poor and thus the model has to be improved. It is suggested that the model is made more flexible in order to reproduce the effects found during the testing. When the FEM has been adapted, it can be correlated again with the test results and no additional modal analysis is necessary.

THIS PAGE INTENTIONALLY LEFT BLANK

V. LIST OF REFERENCES

- [1] D. Sakoda, J. A. Horning and S. D. Moseley, *Naval Postgraduate School NPSAT1 Small Satellite*, 2006.
- [2] D. J. Ewins, *Modal Testing: Theory, Practice and Application*, Second ed., Hertfordshire: Research Studies Press Ltd., 2000.
- [3] Siemens, *NX I-deas Help Files*.
- [4] R. J. Allemang, "The Modal Assurance Criterion - Twenty Years of Use and Abuse," *Sound and Vibration*, August 2003.
- [5] S. Rahn, "Modal Test of a Substructure of NPSAT1," Monterey, 2012.
- [6] Agilent Technologies, *The Fundamentals of Modal Testing*, 1997.
- [7] D. J. Ewins, *Modal Testing: Theory and Practice*, Somerset: Research Studies Press Ltd., 1984.
- [8] J. P. D. Hartog, *Mechanical Vibrations*, McGraw-Hill Book Company Inc., 1956.
- [9] Brüel & Kjaer, *PulseReflex Help Files*.